HNPS Advances in Nuclear Physics

Vol 29 (2023)

HNPS2022

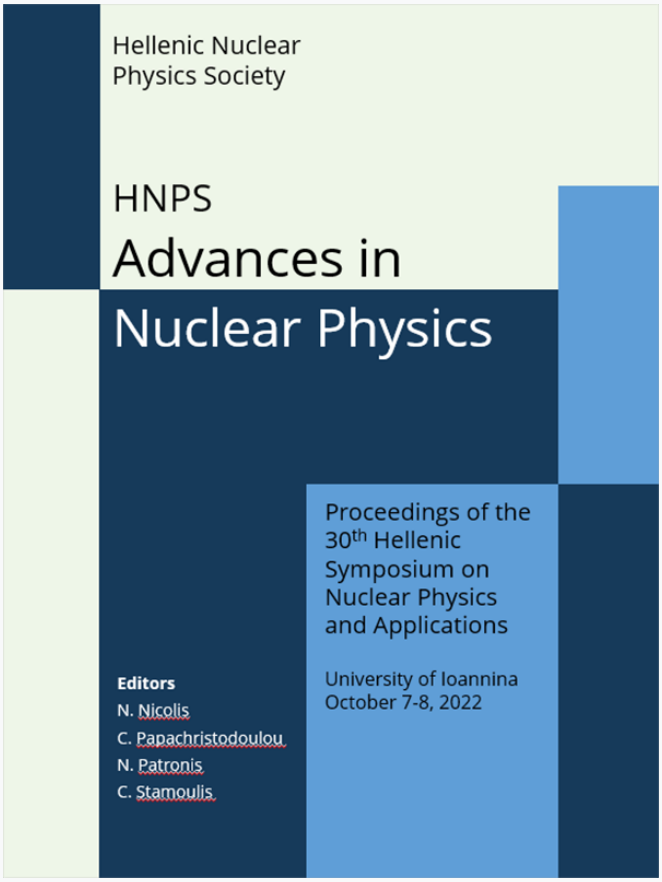

The neutrino floor: a data-driven analysis

Dimitrios K. Papoulias

doi: 10.12681/hnpsanp.5093

To cite this article:

Papoulias, D. K. (2023). The neutrino floor: a data-driven analysis. *HNPS Advances in Nuclear Physics*, *29*, 100–106. https://doi.org/10.12681/hnpsanp.5093

The neutrino floor: a data-driven analysis

D.K. Papoulias*

Department of Physics, National and Kapodistrian University of Athens, Zografou Campus, GR-15772 Athens, Greece

Abstract We revisit the discovery limit of multi-ton direct detection dark matter experiments in the light of recent measurements of the coherent elastic neutrino-nucleus scattering process. Assuming the cross section to be a parameter entirely determined by data instead of using its Standard Model prediction, we exploit the COHERENT CsI and LAr data sets to determine WIMP discovery limits. We point out that the data-driven approach followed in this study is rather advantageous, making the present results to become free from theoretical assumption. We find that CsI (LAr) data lead to an improvement (worsening) of the neutrino floor and fall within the WIMP mass regions where XENONnT and DARWIN have best expected sensitivities.

Keywords neutrino floor, coherent elastic neutrino nucleus scattering, WIMP-nucleus scattering

INTRODUCTION

The dark matter (DM) direct detection program dates back to the early nineties, with the first germanium ionization detectors using few kilogram target material [1]. The latest data leading to the most stringent limits on the DM-nucleon cross section, follow from measurements of order ton-size liquid xenon (LXe) time projection chambers (TPCs) and include the LUX, PandaX-II and XENON1T experiments [2–4]. Measurements on liquid argon (LAr) TPCs, which include DarkSide-50 and DEAP-3600, have placed limits as well, albeit less stringent due to their lower exposures and higher recoil energy thresholds [5, 6]. In the next few years, searches will continue, with LXe TPC experiments paving the way. Future experiments include LZ, XENONnT and ultimately DARWIN, detectors which involve multi-ton fiducial volumes [7–10]. The advent of the multi-ton era implies that DM searches will be subject to irreducible neutrino backgrounds, in particular those emitted in the ^{8}B process of the solar pp chain [11, 12].

Neutrino backgrounds induce coherent elastic-neutrino nucleus scattering (CEνNS) [13] and produce nuclear recoil spectra, which, depending on the WIMP parameter space, can have a strong degeneracy with those expected from spin-independent WIMP interactions. Actually, a full degeneracy is found between ^{8}B solar (atmospheric) neutrinos and a WIMP model defined by a WIMP mass $m_\chi = 6$ (100) GeV and a WIMP-nucleon cross section $\sigma_{n-\chi}=5\times10^{-45}$ cm^2 (10^{-48} cm^2) [12]. This level of degeneracy thus leads to a saturation of the WIMP-nucleon cross section to which a particular experiment can have access. So, in contrast to the background-free paradigm, increasing exposure does not imply a linear improvement of sensitivities but rather a saturation of its discovery limit [11], typically referred to as neutrino floor. Various experimental techniques that enable overcoming the neutrino floor have been discussed in the literature. They include measurements of the WIMP and neutrino recoil spectra tails [15], directionality (see e.g. [16]), measurements with different material targets [15] and annual modulation [17]. However, although feasible in principle, some of them require large exposures and/or further technological improvements. The experimental reach of multi-ton DM direct detection experiments (with no directional capabilities) thus depends crucially on the precision with which WIMP and CEνNS induced events can be predicted. WIMP event rates are subject to astrophysical uncertainties, which depend e.g. on the DM halo model assumed for their calculation. Their impact has been studied in detail in Ref. [18]. CEνNS event rate

* Corresponding author: dk.papoulias@phys.uoa.gr

uncertainties instead can be thought of as being of two types, those associated with neutrino flux normalizations and those associated with the CEνNS cross section. The Standard Model (SM) CEνNS cross section uncertainties are mainly driven by nuclear physics effects, encoded in the weak-charge form factor [18–21]. For solar neutrinos these effects barely exceed ∼ 1%, while for atmospheric neutrinos they can be larger but never exceeding ∼ 10%. For this reason, the neutrino flux normalization uncertainties dominate the determination of the experimental reach a given experiment can have.

The advent of the multi-ton era requires an understanding of the discovery reach beyond that implied by the neutrino flux normalization factors uncertainties. Since the effects of astrophysical uncertainties have been already quantified, and have been proved to have a small effect [18], for this task one should rather focus on the uncertainties in the neutrino sector. In order to do so, one can adopt a data-driven approach or instead consider all possible effects that might have an impact on the discovery potential. This paper aims at exploring both cases for LXe and LAr detectors. By data-driven analysis, we mean using COHERENT data [22–24] to extract the CEνNS cross section along with its uncertainty. The advantage of this approach is that, in such a way, the cross section uncertainty encapsulates all possible effects, including possible new physics contributions, without the need of any further assumption. We also present a more assumption-dependent analysis in which we consider what could be regarded as subleading uncertainties. These include effects related with possible low-energy variations of the weak mixing angle and the unknown value of the xenon point-neutron distribution mean-square radius. Finally, given the precision with which CEνNS has been currently measured, possible new physics effects can have a significant impact too (see for instance [25–31]).

WIMP AND NEUTRINO EVENT RATES

On dimensional grounds, event rates can be estimated to be given by the number of scatterers N_N, the incident particle flux Φ and the interaction probability of the incident particles with the scatterers σ. In terms of these variables, the number of expected events per unit of amount of target material and per time is given by $R \sim N_N \times \Phi \times \sigma$. For DM, astrophysical assumptions on the DM halo model are required to predict the WIMP flux at the detector. As for neutrinos, fluxes fall into three categories: solar, diffuse supernova neutrino background (DSNB) and sub-GeV atmospheric neutrinos. Whether a certain type or component matters or not for a certain detector depends on the energy threshold. In particular, for LXe detectors it is known that only the ^{8}B component of the solar neutrino spectrum matters [12, 16]. Here, however, we consider all components, which allows to extend our analysis to a wider DM mass range.

The CEνNS differential recoil spectrum comes out of a convolution of neutrino fluxes and the CEνNS differential cross section. For the α-th flux component it reads [27]

$$\frac{dR_\nu}{dE_r} = \varepsilon \frac{N_A}{m_{\text{target}}} \int_{E_\nu^{\min}}^{E_\nu^{\max}} \frac{d\Phi_\alpha}{dE_\nu} \frac{d\sigma}{dE_r} dE_\nu \ . \tag{1}$$

Here, ε refers to the exposure in ton·year units, N_A to the Avogadro number in mol^{-1} units, m_{target} to the nuclear target molar mass and $d\Phi_\alpha/dE_\nu$ to the neutrino flux including its normalization (see Table 1). The lower limits of integration are determined by the kinematics of the process. Since xenon has 9 stable isotopes, few of which have substantially large natural abundances, in our analyses we work with averaged nuclear mass and mass number: $m_N = \Sigma_i\, m_i\, X_i$ and $A = \Sigma_i\, A_i\, X_i$, with the sum running over all stable isotopes. The integration upper limit is determined by the flux kinematic tail.

Table 1. *Neutrino flux normalization factors along with their uncertainties as predicted by the B16-GS98 high metallicity SSM [32]*

Neutrino flux components normalizations and uncertainties					
Comp.	Norm. $[\mathrm{cm}^{-2}\cdot\mathrm{s}^{-1}]$	Unc.	Comp.	Norm. $[\mathrm{cm}^{-2}\cdot\mathrm{s}^{-1}]$	Unc.
^{7}Be (0.38 MeV)	4.84×10^{8}	3%	^{7}Be (0.86 MeV)	4.35×10^{9}	3%
pep	1.44×10^{8}	1%	pp	5.98×10^{10}	0.6%
^{8}B	5.25×10^{6}	4%	hep	7.98×10^{3}	30%
^{13}N	2.78×10^{8}	15%	^{15}O	2.05×10^{8}	17%
^{17}F	5.29×10^{6}	20%	DSNB	86	50%
Atm	10.5	20%	—	—	—

The CEvNS differential scattering cross section, determined by a neutral current process, is given by [20]

$$\frac{d\sigma}{dE_r}=\frac{m_N G_F}{2\pi}Q_W^2 F_W^2(q)\left(2-\frac{m_N E_r}{E_\nu^2}\right)\,, \tag{2}$$

where Q_W is the coherent weak charge that quantifies the coupling of the Z gauge boson to the nucleus. It is, therefore, entirely determined by electroweak Z − q couplings, namely [13]

$$Q_W=(A-Z)(g_V^u+2g_V^d)+Z(2g_V^u+g_V^d)\,, \tag{3}$$

with the couplings given by $g_u^V=1/2-4/3\sin^2\theta_W$ and $g_d^V=-1/2+2/3\sin^2\theta_W$. For the weak mixing angle, in our analyses, we use its low-energy value obtained by the RGE extrapolation from the Z scale to $q^2=0$, $\sin^2\theta_W=0.23857$. The cross section in Eq.(2) comes along with the weak-charge nuclear form factor which, combined with the coherent weak charge, determines the q-dependent strength of the Z-nucleus coupling. Throughout the paper, we use the Helm parametrization.

On the other hand, the WIMP-nucleus differential recoil spectrum can be written as [18]

$$\frac{dR_W}{dE_r}=\varepsilon\frac{\rho_0\sigma_{\mathrm{SI}}(q)}{2m_\chi\mu^2}\int_{|\boldsymbol{v}|>v_{\min}}d^3v\,\frac{f(\boldsymbol{v})}{v}\,, \tag{4}$$

where $\rho_0=\rho(R_0)$ ($R_0=8$ kpc) is the local halo DM density, $\sigma_{\mathrm{SI}}(q)$ is the spin-independent momentum-transfer-dependent WIMP-nucleus scattering cross section, m_χ is the WIMP mass and μ is the WIMP-nucleus reduced mass: $\mu=m_\chi m_N/(m_\chi+m_N)$. The integral corresponds to the mean inverse speed and its value is determined by the assumed velocity distribution. The minimum WIMP velocity that can induce a nuclear recoil with energy E_r depends on whether the scattering is elastic or inelastic. For elastic scattering, for which our results apply, one finds $v_{\min}=\sqrt{mN\,Er/2}/\mu$. In scenarios where the WIMP-proton and WIMP-neutron scattering cross sections are equal (spin conserving scenarios, $f_p/f_n=1$), and nucleon form factor q-dependent terms are neglected, $\sigma_{\mathrm{SI}}(q)$ can be written as [32]

$$\sigma_{\mathrm{SI}}(q)=\frac{\mu^2}{\mu_n^2}\left[ZF_p(q)+(A-Z)F_n(q)\right]^2\sigma_{\chi-n}\,, \tag{5}$$

where $\sigma_{\chi-n}$ is the WIMP-nucleon momentum-transfer-independent cross section and μ_n refers to the WIMP-nucleon reduced mass, with $m_n=931.5$ MeV.

The results presented in the following sections are obtained assuming the standard halo model (SHM), which assumes that the local DM halo is dominated by a smooth and virialized component (non-virialized components, such as streams or debris flows, are regarded as subleading), well-described by an isothermal sphere with an isotropic and Maxwellian velocity distribution [18]

$$f(v)=\begin{cases}\frac{1}{N_{\mathrm{esc}}}\left(\frac{3}{2\pi\sigma_v^2}\right)^{3/2}e^{-3\boldsymbol{v}^2/2\sigma_v^2} & \text{for}\quad v<v_{\mathrm{esc}}\,,\\ 0 & \text{for}\quad v>v_{\mathrm{esc}}\,,\end{cases} \tag{6}$$

where σ_v refers to the root-mean-square velocity dispersion and N_{esc} is the normalization factor (see Table 2). For illustration purposes, in Fig. 1 we show the neutrino and WIMP differential recoil spectra expected in the SM (left panel) and in a new physics scenario with a light vector mediator (right panel).

Table 2. *Values for the average, laboratory and escape velocities along with the local halo DM density ρ0 = ρ(R0 = 8 kpc) used in the determination of WIMP discovery limits [32]*

Relevant WIMP related parameters			
v_0 [km/s]	v_{lab} [km/s]	v_{esc} [km/s]	ρ_0 [GeV/cm^3]
220	232	544	0.3

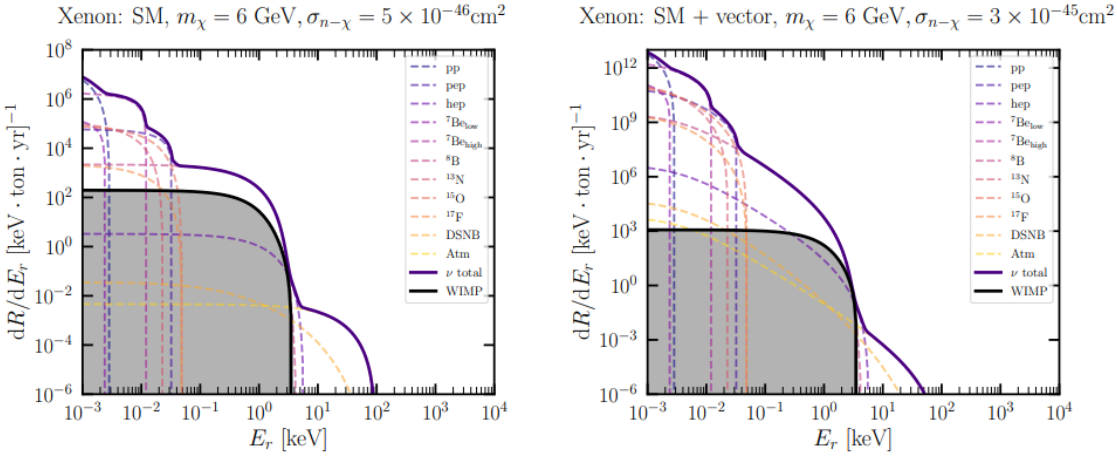

Figure 1. *Left graph: Neutrino and WIMP differential recoil spectra expected in the SM. Right graph: Neutrino and WIMP differential recoil spectra in the presence of a long-range vector interaction [32].*

STATISTICAL METHOD

The general likelihood function we adopt depends on WIMP parameters (m_χ and $\sigma_{\chi-n}$), as well as on the nuisance parameters associated with neutrino fluxes normalization factors (denoted φ_α, with α = 1, · · · , n_ν = 11) and nuisance P, with $P = \{n_\sigma, R, \Theta\}$ (R and Θ refer to the R_n and $\sin^2\theta_W$ nuisance parameters, while n_σ stands for the ratio between the experimentally measured CEvNS cross section and its SM theoretical value) [32]

$$\mathcal{L}(m_\chi, \sigma_{\chi-n}, \Phi, \mathcal{P}) = \prod_{i=1}^{n_{bins}} P(N^i_{Exp}, N^i_{Obs}) G(\mathcal{P}_i, \mu_{\mathcal{P}_i}, \sigma_{\mathcal{P}_i}) \times \prod_{\alpha=1}^{n_\nu} G(\phi_\alpha, \mu_\alpha, \sigma_\alpha) \ , \quad (7)$$

with Φ = (φ_1, · · · , φ_{nv}). For the data-driven analysis, n_{bins} is dictated by COHERENT data, so n_{bins} = 12 for CsI [22] and n_{bins} = 3 for LAr [24]. $P(x, n)$ and $G(x, \mu, \sigma)$ are Poisson and Gaussian probability distribution functions, respectively. This means that N_{Obs} is assumed to be a Poissonian random variable and that the nuisance parameters follow instead Gaussian distributions that parametrize their uncertainties. To set discovery limits, one defines a null hypothesis H_0 (CEvNS background only) and an alternative hypothesis H_1, which involves the WIMP signal plus the CEvNS background. The likelihood function in Eq.(7) is then specialized for the two cases: L_0 for H_0 and L_1 for H_1. In both, $N^i_{Obs} = \sum_a N^i_\nu(\Phi_a, P_i) + N^i_W(P_i)$, where N^i_{Obs} refers to the total number of "observed" events in the i-th bin in a toy experiment defined by a parameter space point (m_χ , $\sigma_{\chi-n}$) and the neutrino flux normalization factors, as well as P fixed to their means. For L_0 and in the i-th bin, the "expected" number of events is given by $N^i_{Exp} = \sum_a N^i_\nu(\Phi_a, P_i)$, where the neutrino flux normalizations, as well

as P are parametrized in terms of their nuisance variables. For L_1, we make use of the Asimov data set (i.e. $N^i_{Exp} = N^i_{Obs}$) [18].

For each parameter space point, one evaluates the likelihood ratio (test statistics) $\lambda(0) = L_0/L_1$ which quantifies the disagreement between the null and alternative hypotheses (e.g. significance of the WIMP signal), through the equivalent significance defined according to $Z = \sqrt{-2 \ln \lambda(0)}$. The discovery limit then follows by finding the smallest WIMP cross section for which 90% of the experiments have a WIMP signal above 3σ. In terms of the equivalent significance, this translates into $Z \geq 3$.

RESULTS AND DISCUSSION

To proceed, we first extract from the COHERENT CsI [22] and LAr [24] data the CEνNS cross section central values along with their standard deviations. Note that the CsI data are directly applicable to xenon, since both nuclides have about the same average mass and atomic numbers. To this purpose, we weigh the theoretical SM value of the CEνNS differential cross section with a multiplicative factor n_σ and use a spectral χ^2 test to fit n_σ in each recoil energy (see the Apppendix of Ref. [32] for details). Assuming that the CEνNS differential cross section uncertainty is fully encoded in a multiplicative factor, is the most simple approach one can adopt. Given the quality of the data sets, the uncertainty could be assumed to be energy-dependent. However, modeling such an energy-dependent uncertainty seems to us more arbitrary (there is a few number of functions one could use) than assuming a flat uncertainty. For the data-driven analysis with COHERENT CsI data, we use 12 bins starting at 7 photoelectrons (PE) and extending up to 29 PE (PE = 1.17 Er/keV$_{nr}$), while for the LAr dataset, we use three bins starting at 5 keV$_{ee}$ and up to 25 keV$_{ee}$. Note that in the definition of the χ^2 test, to extract the n_σ factors, systematic errors associated to neutrino flux and form factor uncertainties (for a detailed discussion see e.g. Refs. [20,21]) have been included as nuisance parameters. The results presented in Fig. 1 thus encode only uncertainties due to the cross section (indirect) measurement.

The datasets available for the CsI and LAr COHERENT detectors provide spectral information on the measured number of CEνNS events and their uncertainties. Under the assumption that the experimental cross section is proportional to its theoretical prediction, the COHERENT collaboration has already provided a determination of the measured CEνNS cross section on argon, as $\sigma_{meas} = N_{meas}/N_{th}\ \sigma_{th}$ [24], where N_{meas} and N_{th} are the total number of measured and theoretical events, respectively. Motivated by the latter, here we perform a similar analysis which in our case is applied independently for each energy bin by considering $\sigma^i_{\rm meas} = n^i_\sigma\ \sigma^i_{\rm th}$. Following this approach, we extract the measured cross section along with its uncertainty for both CsI and LAr datasets. For the case of CsI, we adopt the χ^2 function [22]

$$\chi^2_i = \left[\frac{N^i_{\rm exp} - (1+\alpha)N^i_{\rm meas}(n^i_\sigma) - (1+\beta)B^i_{0\rm n}}{\sigma^i_{\rm stat}}\right]^2 + \left(\frac{\alpha}{\sigma_\alpha}\right)^2 + \left(\frac{\beta}{\sigma_\beta}\right)^2, \tag{8}$$

where α and β are nuisance parameters which account for the uncertainty on the rate with $\sigma_\alpha = 28\%$ and on the prompt neutron background B_{0n} with $\sigma_\beta = 25\%$, respectively ($\sigma^i_{\rm stat}$ is the statistical uncertainty in the i-th bin). For the case of LAr, we focus on the analysis-A of COHERENT [23] and we follow the χ^2 function [24]

$$\chi^2_i = \frac{\left(N^i_{\rm exp} - \alpha N^i_{\rm meas}(n^i_\sigma) - \beta B^i_{\rm PBRN} - \gamma B^i_{\rm LBRN}\right)^2}{\left(\sigma^i_{\rm exp}\right)^2 + \left[\sigma_{\rm BRNES}\left(B^i_{\rm PBRN} + B^i_{\rm LBRN}\right)\right]^2} + \left(\frac{\alpha-1}{\sigma_\alpha}\right)^2 + \left(\frac{\beta-1}{\sigma_\beta}\right)^2 + \left(\frac{\gamma-1}{\sigma_\gamma}\right)^2. \tag{10}$$

Exploiting this determination of the uncertainties on the CEνNS cross section from COHERENT data, we then compute the WIMP discovery limits. We use the general definition of the likelihood function

in Eq.(7) along with the results depicted in Fig. 2. This implies that the regions that can be covered correspond to those affected by DSNB and sub-GeV atmospheric neutrino backgrounds (heavy WIMP masses). The results are displayed in Fig. 3, using CsI (LAr) data in the left (right) panel. In the analysis with CsI data, one can see that, in general, compared with the SM expectation (solid curves), WIMP discovery limits improve. A closer inspection to the left graph in Fig. 2 allows to understand this behavior. Except for bin number 12, the measured CEvNS cross section (central values) is smaller than the SM expectation, thus resulting in a background depletion which becomes more visible with increasing exposure. However, for low WIMP masses, $m_\chi \leq 20$ GeV, our likelihood analysis tends to favor the maximum cross section values, hence leading to a poorer sensitivity compared to the pure SM case. Results derived using the LAr data behave the other way around. The data trend is that of a measured CEvNS cross section exceeding its SM expectation, as can be seen in the right graph of Fig. 2. Departures, however, are not substantial and thus the enhancement of the background is not that large. As a result, discovery limits are only slightly worsen, as shown in the left graph in Fig. 3.

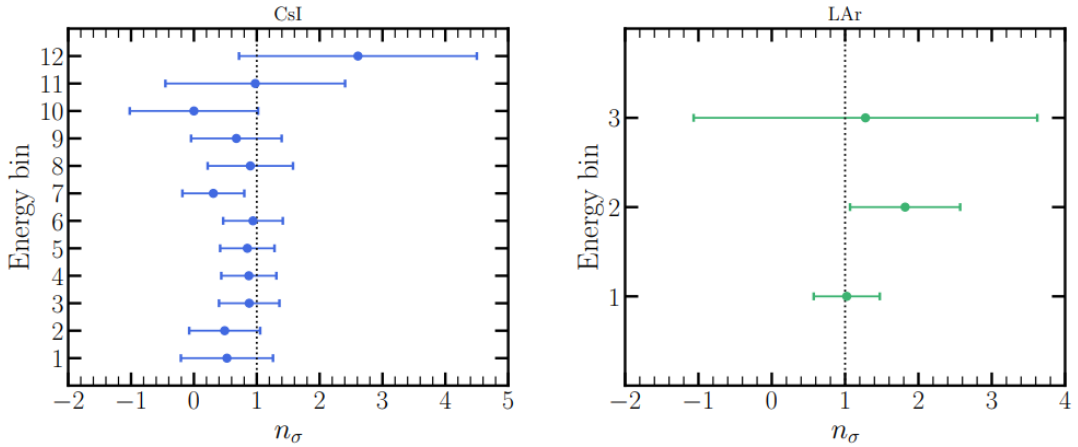

Figure 2. *Experimentally measured CEvNS cross section normalized to the SM prediction (n_σ), extracted from COHERENT CsI and LAr data. Results in each recoil energy bin indicate the central value (mean) along with its uncertainty (1σ) [32].*

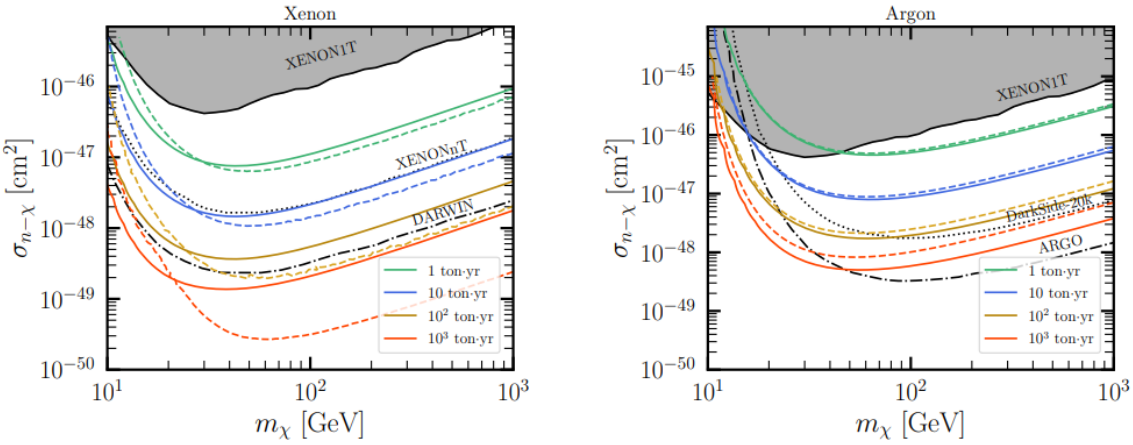

Figure 3. *WIMP discovery limits obtained using the CEvNS cross section measurements at COHERENT with the CsI (left graph) and LAr (right graph) detectors (dashed curves). In addition to the nuisance parameters due to uncertainties on the neutrino flux normalizations, the results include bin-dependent nuisance parameters associated with the CEvNS cross section uncertainty as shown in Fig. 1. The current constraint set by XENON1T is shown in both panels. Moreover, we show as for comparison future sensitivities expected at LXe experiments XENONnT and DARWIN (left panel) and at LAr experiments DarkSide-20k and ARGO (right panel) [32].*

CONCLUSIONS

With the advent of the DM multi-ton detectors era in mind and with well-established measurements of the CEνNS process by the COHERENT collaboration, we have reconsidered the case of WIMP discovery limits. We have adopted, for the first time, a data-driven analysis in which we have treated the CEνNS cross section as a parameter entirely determined by experimental data. Using this approach, while taking into account neutrino flux uncertainties, we have derived WIMP discovery limits using the CsI and LAr COHERENT data sets. Our results are free from theoretical and phenomenological assumptions. They are also of particular interest for future experiments XENONnT, DARWIN, DarkSide-20k and ARGO, as they fall in the region where these experiments will have maximum sensitivities. Finally, we point out that searches for WIMPs using forthcoming multi-ton detector technologies require a precise understanding of WIMP discovery limits. In our view, this calls – ideally – for the most assumption-free determination of the effects of the neutrino background, for the inclusion of known sub-leading effects and the consideration of possible new physics effects.

References

[1] L. Baudis, Phys. Dark Univ. 1, 94 (2012)
[2] LUX Collaboration, D. S. Akerib et al., Phys. Rev. Lett. 116, 161301 (2016)
[3] PandaX-II Collaboration, X. Cui et al., Phys. Rev. Lett. 119, 181302 (2017)
[4] XENON Collaboration, E. Aprile et al., Phys. Rev. Lett. 123, 251801 (2019)
[5] DarkSide Collaboration, P. Agnes et al., Phys. Rev. D 98, 102006 (2018)
[6] DEAP Collaboration, R. Ajaj et al., Phys. Rev. D 100 no. 2, 022004 (2019)
[7] LUX-ZEPLIN Collaboration, D. S. Akerib et al., arXiv:1802.06039 [astro-ph.IM]
[8] XENON Collaboration, E. Aprile et al., JCAP 1604, 027 (2016)
[9] DARWIN Collaboration, J. Aalbers et al., JCAP 1611, 017 (2016)
[10] XENON Collaboration, E. Aprile et al., JCAP 11, 031 (2020)
[11] L. E. Strigari, New J. Phys. 11, 105011 (2009)
[12] J. Billard, L. Strigari, and E. Figueroa-Feliciano, Phys. Rev. D89, 023524 (2014)
[13] M. Abdullah, et al., e-Print:2203.07361 [hep-ph]
[14] J. B. Dent, B. Dutta, J. L. Newstead, and L. E. Strigari, Phys. Rev. D93, 075018, (2016)
[15] F. Ruppin, J. Billard, E. Figueroa-Feliciano, and L. Strigari, Phys. Rev. D90, 083510, (2014)
[16] S. E. Vahsen, C. A. J. O'Hare, and D. Loomba, Ann. Rev. Nucl. Part. Sci. 71, 189 (2021)
[17] J. H. Davis, "Dark Matter vs. Neutrinos: JCAP 1503, 012 (2015)
[18] C. A. O'Hare, Phys. Rev. D94, 063527 (2016)
[19] D. Aristizabal Sierra, J. Liao, and D. Marfatia JHEP 06, 141 (2019)
[20] D. K. Papoulias, T. S. Kosmas, R. Sahu, V. K. B. Kota, and M. Hota Phys. Lett. B 800, 135133 (2020)
[21] M. Hoferichter, J. Menéndez, and A. Schwenk, Phys. Rev. D 102 , 074018 (2020)
[22] COHERENT Collaboration, D. Akimov et al., Science 357, 1123 (2017)
[23] COHERENT Collaboration, D. Akimov et al., arXiv:1804.09459 [nucl-ex]
[24] COHERENT Collaboration, D. Akimov et al., Phys. Rev. Lett. 126, 012002 (2021)
[25] B. Dutta, S. Liao, L. E. Strigari, and J. W. Walker, Phys. Lett. B773, 242 (2017), arXiv:1705.00661 [hep-ph]
[26] E. Bertuzzo, F. F. Deppisch, S. Kulkarni et al., JHEP 04, 073 (2017)
[27] D. Aristizabal Sierra, N. Rojas, and M. H. G. Tytgat, JHEP 03, 197 (2018)
[28] C. Bœhm, D. G. Cerdeño, P. A. N. Machado et al., JCAP 01, 043 (2019)
[29] R. Essig, M. Sholapurkar, and T.-T. Yu, Phys. Rev. D 97, 095029 (2018)
[30] P. B. Denton, Y. Farzan, and I. M. Shoemaker, JHEP 07, 037 (2018)
[31] D. Aristizabal Sierra, B. Dutta, S. Liao, and L. E. Strigari, JHEP 12, 124 (2019)
[32] D. Aristizabal Sierra, V. De Romeri, L.J. Flores, D.K. Papoulias. E. Strigari, JCAP 01, 055 (2022)